Evaluating North American Mountain Snowpack Extent in Regional Climate Models Using MODIS Satellite Imagery

Abstract

Mountain snowpack is a vital source of water for ecosystems, has a significant influence on the occurrence of wildfires, and provides water resources for billions of people globally. Despite the implications of climate change on mountain snowpack, we have few reliable ways of estimating global snowpack extent. In response to the lack of accurate methods of estimating mountain snowpack, Wrzesien et al. (2018) presented an estimate of snowpack extent for eleven North American mountain ranges using regional climate model (RCM) simulations. This research evaluates these model estimates using remote sensing imagery from the NASA Terra MODIS satellite instrument, providing further analysis of the usefulness of RCMs in estimating mountain snowpack. In comparison to MODIS, the RCM simulations generally perform well for most of the year for most ranges, though there is a trend towards spring overestimation of snow cover extent. Spatially, there is no clear trend in the performance of the RCM simulations. Further analysis using other remote sensing datasets could provide more insight into the ability of RCMs to accurately simulate mountain snowpack extent.

Introduction

Mountains act as natural reservoirs, storing snow as it accumulates throughout the winter season in the form of snowpack (Vivrioli et al. 2007). As temperatures rise in the spring and summer, snowpack melts, providing a critical source of runoff for downstream environments. Mountain snowpack has both societal and ecological importance. Over a billion people rely on

spring runoff from mountains for water resources globally (Dozier et al. 2016). The seasonal snowmelt cycle also has a significant influence on the occurrence of wildfires (Gergel et al. 2017) and supplies necessary moisture for alpine ecosystems late into the melt season (Bjork and Molau, 2007).

Warming temperatures due to global climate change are predicted to affect snow-dominated mountain basins disproportionately due to fundamental changes in the seasonal snowmelt cycle (Barnett et al. 2005). As temperatures warm, snow will likely melt earlier in the season, leading to significant declines in spring snowpack levels (Musselman et al. 2017). In the mid-elevations in some regions, such as the Sierra Nevada of California, rain is predicted to replace snow during the winter months, further reducing snow accumulation (Sun et al. 2018). Spring snowpack loss has already been widely observed across western North America and can be attributed to regional-scale warming of the climate (Kapnick et al. 2011, Zeng et al. 2018, Mote et al. 2005). These changes increase the risk of water scarcity in snowmelt-dominated regions (Barnett et al. 2005), increase the risk of wildfires in the western United States (Westerling et al. 2006), and threaten the survival of vulnerable snowbed ecosystems (Bjork and Molau, 2018).

Despite the threat that climate change poses to the seasonal snowmelt cycle, we have few accurate ways of quantifying the spatial distribution of mountain storage globally (Dozier et al. 2016). Surface measurement networks rarely cover high elevations and are too sparse to provide comprehensive and accurate estimates of mountain snowpack (Dozier et al. 2016). In North America, measurement networks are generally limited to the low elevations in the mid-latitudes and urban areas (Robinson et al. 1993). Furthermore, ground snow measurements are influenced by local effects, such as microclimatic and topographic variations, leading to variability in

measurements between different sites (Stewart, 2009). Global climate models (GCMs) have been widely used to assess future changes to the climate, including spatial changes in runoff and snowmelt (Adam et al. 2009). While GCMs are useful for widescale analyses, their resolutions are currently too coarse to accurately represent areas with complex topography such as mountains (IPCC 2013). The lack of baseline estimates of global mountain snowpack will make it difficult or impossible to quantify future changes due to a warming climate (IPCC 2013).

In response to the lack of large-scale estimates of mountain snowpack, Wrzesien et al. (2018) presented an estimate of mountain snow water equivalent (SWE) for eleven North American ranges using regional climate model (RCM) simulations. These simulations were done for a single representative water year between 2001 to 2014 for each range, thereby reducing computational costs while still providing a representative estimate of mountain SWE (Wrzesien et al. 2018). The estimates were compared to in-situ observations and satellite gravimetry data to evaluate their reasonableness (Wrzesien et al. 2018).

The goal of this research is to further evaluate Wrzesien et al. 2018's RCM estimates of North American mountain snowpack by examining patterns in snow covered fraction (SCF). SCF, the fractional snow cover of each grid cell, can be measured using satellite remote sensing instruments. In this study, we compare RCM SCF estimates to data from the Moderate Resolution Imaging Spectroradiometer (MODIS) instrument on the NASA Terra satellite. The MODIS snow-cover mapping product, MOD10A1, provides an estimate of snow cover per pixel per day. This research uses a binary estimate of snow cover per pixel ('snow', 'no snow') derived from the MOD10A1 SCF estimate.

Past comparisons of RCM simulations of snow cover to MODIS imagery have been limited to smaller domains, such as the Sierra Nevada or the Colorado Rockies (Wrzesien et al.

2015; Minder et al. 2016). This research aims to evaluate RCM simulations for the entirety of North American mountain ranges using a satellite-based SCF product. Furthermore, this analysis addresses the usefulness of RCMs in estimating mountain snow extent, which is necessary for understanding how mountain snowpack is likely to change in the future.

Data and Methods

Data:

WRF:

We use SCF estimates from the Weather Research and Forecasting Regional Climate Model (WRF) version 3.6.1 (Skamarock et al. 2008), as modeled by Wrzesien et al. (2018). WRF was coupled to the Noah land surface model (LSM) with multiparameterization options (Noah-MP) (Niu et al. 2011), with ERA-Interim providing the meteorological conditions at the boundary (Dee et al. 2011). Wrzesien et al. (2018) chose the following physics options when running WRF: the Thompson et al. 2004 cloud microphysics scheme, the Rapid Radiative Transfer Model longwave scheme (Mlawer et al. 1997), the Dudhia shortwave scheme (Dudhia, 1989), the Yonsei University planetary boundary layer scheme (Hong et al. 2006), and the modified Kain-Fritsch convective parameterization for the two outer domains (Kain, 2004; Kain and Fritsch, 1990, 1993).

Unlike the original Noah LSM, Noah-MP divides snowpack into up to three distinct layers depending on total snow depth, allowing for more accurate simulation of snowpack temperature (Etchevers et al. 2004, Niu et al. 2011). A snowfall interception model incorporates leaf area index (LAI) to account for canopy interception of snow (Niu and Yang, 2004).

Including canopy interception can lead to a smaller estimated snow cover on the ground (Niu et al. 2011), thus affecting SCF estimates. Noah-MP calculates SCF using Equation 1, where h_{sno} represents snow depth, ρ_{sno} represents snow density, ρ_{new} represents fresh snow density, m is a scalable melt factor, and $z_{0,g}$ is the ground roughness length (Niu and Yang, 2007; Niu et al. 2011). The inclusion of snow density accounts for variations in SCF between the accumulation and melt season due to patchy snow, even when grid averaged snow depth may be the same during both periods (Niu and Yang, 2007). This SCF calculation results in values up to 40% greater than previous modeling estimates (Niu and Yang, 2007).

$$SCF = tanh\left(\frac{h_{sno}}{2.5 z_{0,g}(\rho_{sno}/\rho_{new})^{m}}\right) \qquad Equation\ 1$$

Wrzesien et al. (2018) ran WRF for eleven North American mountain ranges (Figure 1). Because of computational constraints associated with running a climate model for the entirety of North America for a 30-year period, Wrzesien et al. (2018) chose a representative water year to model for each range to provide a baseline climatology. Water years between 2001 and 2014 were chosen for each respective range by comparing climatological snow water storage (SWS) estimates from two reanalysis datasets and selecting the year closest to the climatological average (Wrzesien et al., 2018); SWS was calculated by multiplying SWE by grid cell area to estimate the volume of water stored in snowpack. The simulations were run for the first 293 days of each water year, representing October through mid-July. Extents of the ranges themselves were chosen based on the mountain classification by Kapos et al. (2000) using elevation, slope, and local relief (Wrzesien et al. 2018). Past research demonstrated that resolutions of less than 10 km are necessary to accurately simulate mountainous orographic precipitation processes (Ikeda et al. 2010; Minder et al. 2016; Wrzesien et al. 2018). In this study, WRF simulations at a resolution of 9 km are used.

Further information on the representative water years, mountain range bounds, and simulations used in this study can be found in Wrzesien et al. (2018). WRF SWS data are available for download at the National Snow and Ice Data Center (Wrzesien and Durand, 2018).

MODIS Snow-Covered Area:

The MODIS instrument is found on the NASA Terra satellite. Terra follows a circular sun-synchronous polar orbit with a period of 99 minutes, allowing MODIS to see the entirety of the planet every 1-2 days (NASA). The MODIS MOD10A1 snow cover product is currently on its sixth release (Hall and Riggs, 2016). MOD10A1 Version 6 provides daily global snow cover estimates at 500 m resolution from July 2002 to the present (Hall and Riggs, 2016). MOD10A1 identifies snow-covered land using radiance data from the MODIS instrument using the NDSI, a measure of the magnitude of difference between reflectance in a visible band (VIS) and a shortwave infrared band ($SWIR$) (Equation 2) (Nolin, 2010). MOD10A1 uses MODIS band 4, the green band (0.545-0.565 μm), as VIS and band 6 (1.628-1.652 μm) as SWIR (Riggs and Hall, 2016).

$$NDSI = \frac{VIS - SWIR}{VIS + SWIR} \qquad Equation\ 2$$

The NDSI uses snow's characteristically high visible reflectance and low shortwave infrared to calculate snow presence on the surface. NDSI values range from -1.0 to 1.0, with any values greater than 0 representing some snow cover, and 1.0 representing the maximum amount of snow cover possible. The greater the difference between the visible and shortwave infrared bands, the greater the NDSI (Riggs et al. 2016). NDSI is most effective at detecting snow when there are clear skies, good viewing geometry and solar illumination, and at least several centimeters of snow accumulation (Riggs et al. 2016). Because NDSI relies on visible light,

MOD10A1 does not provide data when natural light is limited, resulting in sparse data availability in the winter months at high latitudes. Pixels affected by clouds, shadows, limited light, or other errors resulting in no data availability are classified as null pixels; in this study, only non-null pixels for each day are analyzed. MOD10A1 Version 6 is available to freely download via the National Snow and Ice Data Center and is provided with a cloud mask and night mask overlaid.

The Version 6 NDSI is an estimate of snow cover comparable to the fractional snow cover estimates provided in previous MOD10A1 releases. However, areas with 100% snow cover will not necessarily have an NDSI of 1.0 because of forest canopy and solar geometry (Riggs et al. 2016). Forest cover both obscures hidden snow under the canopy and adds to pixel reflectance, reducing NDSI in vegetated areas (Nolin, 2010; Rittger et al. 2013). This is demonstrated in Figure 2, where the MOD10A1 NDSI for the Alaska range in early February shows lower values across the range compared to SCF. The MOD10A1 NDSI snow cover can be converted to a snow cover fraction estimate, comparable to previous MOD10A1 versions, using Equation 3, which is based on an empirical regression relationship between fractional snow cover and NDSI (Salomonson and Appel, 2004).

$$SCF = -0.01 + 1.45 \cdot NDSI \qquad Equation\ 3$$

Previous versions of MOD10A1 SCF have been shown to underestimate snow cover due to vegetation effects (Rittger et al. 2013). For this reason, a binary classification ('snow', 'no snow') was applied to the SCF. A binary MODIS classification scheme has been shown to agree reasonably well with satellite-based snow cover products and in-situ measurements in other studies (Parajka and Blosch, 2012; Parajka et al. 2006; Simic et al. 2004; Maurer et al. 2002; Klein and Barnett, 2003). These studies have demonstrated that MODIS has the lowest

accuracies in forested areas and during periods of snowmelt due to patchy snow cover. Rittger et al. (2013) showed that MOD10A1 Version 5 failed to identify snow in two North American mountainous regions, the Sierra and Upper Rio Grande, during times of snowmelt.

Some of these issues have been resolved or improved upon in MOD10A1 Version 6. Version 6 has an increase in snow-cover detection accuracy, particularly for mountain ranges in the Northern Hemisphere during spring and summer, compared to earlier versions of MOD10A1 (Riggs et al. 2017). This is largely because the Version 6 update fixes an error with the surface temperature screen; previously, the screen was applied blindly to all pixels with a temperature greater than 283 K, leading to some mixed pixels in mountain regions being labeled as no snow, even when snow was present (Riggs et al. 2017). In Version 6, the screen is only applied to pixels below 1300 meters in elevation. Though MOD10A1 is an imperfect data set, it is one of only a few daily SCF datasets available that cover both the geographic ranges and water years analyzed in this study at a relatively fine spatial scale. Taking these limitations into account, MOD10A1 has still been shown to be a useful tool for comparison, and we therefore used it in this study.

While past research using MODIS snow cover data and previous MOD10A1 versions have used a binary threshold of 0.4 NDSI to determine snow versus no snow, this threshold (approximately 50% fractional snow cover) can lead to losses in snow detection (Riggs et al. 2017). Wrzesien et al. (2015) instead used a threshold of 0.15 (15%) to determine snowy pixels when working with another MODIS snow cover product, the MODIS Snow-Covered Area and Grain Size (MODSCAG) historical data set. Furthermore, Rittger et al. (2013) demonstrated that a 0.15 binary threshold applied to MOD10A1 Version 5 data resulted in precision and recall

statistics of greater than 0.9 for two North American mountain regions. In this study, the 0.15 threshold was applied to the MOD10A1 data.

Methods:

The Wrzesien et al. (2018) WRF simulations of SCF and the MOD10A1 daily SCF data were averaged for each representative water year for each range using a 7-day moving average to fill in any missing data (null pixels). The 0.15 snow cover threshold was applied to determine binary snow coverage. To compare WRF and MOD10A1 SCF of each range temporally, the number of snow-covered pixels per day were summed and then divided by the total number of non-null pixels, resulting in daily SCF estimates for each range and water year. This SCF was presented in values ranging from 0% (no snow cover) to 100% (total snow cover). For comparison, the MOD10A1 and WRF SCFs of each range were treated like absolute numbers, and all comparisons considered MOD10A1 SCF to be the truth. For example, a day with a MOD10A1 SCF of 50% and a WRF SCF of 60% would be considered 10 SCF percentage points overestimated. The daily SCF estimates were further analyzed by season to determine any trends in the WRF SCF classification in comparison to MOD10A1.

For spatial comparison, the MOD10A1 binary SCF was scaled from 500 m resolution to the coarser 9 km resolution of WRF by aggregating the nearest pixels to the WRF grid. Three dates were chosen from each range to represent the early-, mid-, and late-season of the spring and summer melt period. The early season date was chosen as the date with the highest binary SCF after February 3rd for each range, with February representing the earliest month of the melt season. The mid- and late-season dates represent the dates with 66% and 33% remaining snow of the early-season date, respectively. Difference plots were created for each range; each pixel was assigned a value depending on whether it was classified as snow by both WRF and MOD10A1

(true positive, TP), by only WRF (false positive, FP), by only MOD10A1 (false negative, FN), or by neither (true negative, TN). A confusion matrix table for the early-, mid-, and late-season dates was made, with each value representing the percent of the total classified pixels for that date.

Results

Time Series Comparison:

Of the eleven ranges analyzed in this study, WRF overestimates SCF in comparison to MOD10A1 for seven ranges (Figure 3). WRF underestimates SCF for the Coast Range (62% of days underestimated), the Great Basin (61%), the Mackenzie Mountains (83%), and the Torngat Mountains (70%). However, this comparison exaggerates the disagreement between WRF and MOD10A1 by assuming that if their estimates are not identical, they are in disagreement. In the Great Basin range, for example, 62% of the underestimates are less than 0.1 SCF percentage points lower than MOD10A1.

When we instead consider the days where WRF is within 5 SCF percentage points of the MOD10A1 SCF estimate as "in agreement", the only ranges where WRF underestimates SCF more than it overestimates SCF are the Coast and Mackenzie (26% and 18% of days underestimated compared to 11% and 4% of days overestimated, respectively). In these ranges, WRF and MOD10A1 agree 63% and 78% of the time, respectively. The majority of WRF's underestimations for the Coast range happen during the fall (October-November, 44%) and the winter (December-January-February, 44%). For the Mackenzie, almost all (94%) of its underestimates take place in the spring (March-April-May).

Of the nine ranges which WRF overestimates more than underestimates in comparison to MOD10A1, two are overestimated for the majority of the time period (defined greater than 50% of the days; the Appalachians, 72% of the time, and the Cascades, 61% of the time). For the Appalachians, WRF is in agreement with MOD10A1 18% of the time, and only underestimates SCF on one out of 293 days in the water year. For seven of these ranges, WRF and MOD10A1 are in agreement for the majority of the period (Alaska, 80%; American Rockies, 61%; Brooks, 85%; Canadian Rockies, 53%; Great Basin, 62%; Sierra, 64%; Torngat, 72%). Of these ranges, only the Sierra and Great Basin have more than 6% of their days underestimated by WRF.

When WRF overestimates SCF, it tends to do so on a seasonal basis. For the Alaska, American Rockies, Brooks, Canadian Rockies, Cascades, and Torngat ranges, more overestimated days take place during the spring and summer than during any other season. The Alaska, Brooks, and Torngat ranges are primarily overestimated in during the summer (June-July) (80%, 77%, and 50% of overestimated days, respectively), while the Canadian Rockies are evenly split between spring and summer (36% and 33% of overestimated days, respectively). For the American Rockies and Cascades, most of the days that WRF overestimates SCF take place in the spring (48% and 49%), closely followed by the winter season (45% and 23%, respectively). The Great Basin and Sierra ranges have the majority of their overestimated days in the winter, though there is no clear seasonal pattern for either range. For the Appalachians, in particular, WRF overestimates SCF consistently throughout the entire water year.

Spatial Comparison:

There is no clear spatial relationship in differences between WRF and MOD10A1 for any of the ranges, though WRF tends to overestimate snow cover along the boundaries of the mountain ranges. Based on Table 1, we can divide the ranges into three categories: those that show WRF overestimates SCF across the three dates, or at least one date has a significant overestimation (Alaska, Appalachian, Canadian Rockies, Cascades, and Great Basin), those that show WRF underestimates throughout (Coast, Mackenzie), and those with no clear pattern (American Rockies, Brooks, Sierra). These groupings differ from the patterns observed in the time series analysis. While the American Rockies, Brooks, and Sierra time series comparisons suggest WRF overestimates SCF, the selected dates for the spatial comparison (based on percentage of snow cover remaining) do not capture this trend. For the American Rockies and the Sierra, this is largely because WRF and MOD10A1 SCF follow similar trends across the water year, and the dates chosen happen to show both overestimates and underestimates of SCF. For the Brooks range, WRF's overestimation is concentrated in the summer season, and therefore missed in the spatial comparison.

Of the ranges that WRF overestimates snow cover fraction, three (Alaska, Appalachian, and Canadian Rockies) have above 85% snow cover agreement for the early season date, resulting in low FPs and FNs (Table 1). Spatially, when WRF misclassifies pixels as snow in the Canadian Rockies, Cascades, and Great Basin ranges, it tends to do so on the peripheries of the ranges; both WRF and MOD10A1 agree that the center of the range is snow covered (Figures 8, 9, 11). There is no trend in the geographic regions (north, south, east, or west) of the overestimated boundaries. The Cascades, for example, have FPs concentrated along the southern periphery of the range during the mid-season date and along the northern periphery of the range during the late season date (Figure 9). In the Appalachians, the early-season date displays FNs in

the southern portion of the range almost entirely; the mid-season date is scattered, and the late-season date is almost entirely FPs (Figure 6). The Alaska range has FNs in the central and northern parts of the range during the mid-season date (Figure 4). These regions reverse to FP in the late-season date. There is no clear indication that FNs or FPs happen along the periphery for the Alaska range.

The Coast and Mackenzie ranges are unique among all the ranges in that WRF underestimates snow cover consistently for both the mid- and late-season dates (Table 1). Both have similar spatial patterns for FNs (Figures 10, 12). On the early-season date, the Mackenzie range is nearly 100% snow-covered (FNs are present, but represent less than 1% of the pixels), while the Coast range is 94% TP. On the mid- and late-season dates for both ranges, TPs remain primarily in the center of the ranges. FNs and FPs are located around the peripheries of the ranges and scattered throughout the center of the southern tip of the Coast range.

Of the ranges with no clear trend in snow cover classification across the three dates, the American Rockies and Brooks ranges also show no consistent spatial pattern of misclassified pixels (Figures 5, 7). On the early-season date, the American Rockies has FPs scattered throughout, but mainly located in the southern portion. The Brooks, in contrast, is entirely TPs, similar to other high-latitude ranges in the early-season. On the mid- and late-season dates, FNs are scattered throughout the American Rockies, while FPs are equal in number, but more concentrated together. In the Brooks range, FNs and FPs are also relatively close to each other for both mid- and late-season dates. On the mid-season date, FNs are grouped together along the periphery of the mountain range, while FPs are scattered throughout and grouped in the southern portion. On the late-season date, FNs and FPs are equal in number and grouped together; there is no trend for misclassifications along the periphery. In contrast, the Sierra range remains TP

throughout the center of the range on all three dates. TPs and TNs, in relatively equal proportions, are scattered along the periphery (Figure 13).

Discussion

Based on the analysis of the time series comparison, WRF and MOD10A1 are in agreement (within +/- 5 SCF percentage points of each other) for the majority (defined as more than 50%) of the water year for nine out of eleven ranges (Figure 3). In the two exceptions, the Appalachians and the Cascades, WRF overestimates snow cover in comparison to MOD10A1 for the majority of the year. There are no ranges in which WRF underestimates SCF for >50% of the year, and only two ranges, the Mackenzie and Coast ranges, show an underestimation trend on the early-, mid-, and late-season dates. Therefore, while WRF does overestimate snow cover in comparison to MOD10A1, WRF is in agreement with MOD10A1 for most of the water year for most ranges.

Seasonally, the time series comparison indicates a spring and summer trend for WRF overestimation of snow cover. Six out of eleven ranges (the Alaska, American Rockies, Brooks, Canadian Rockies, Cascades, and Torngat ranges) have more overestimated days in the spring and summer than in any other season. Of these six ranges, the majority of four (Alaska, Brooks, Canadian Rockies, and Torngat) are located north of 50 degrees latitude and remain at, or, in the case of the Canadian Rockies, just below 100% snow cover during the entirety of the winter season. For these ranges, both the spring and summer seasons represent snowmelt periods. Spatially, there is no clear trend of over or underestimating snow cover on the windward/leeward side of any range; there is, however, an indication that FPs and FNs tend to occur along the

boundary of TPs within ranges, usually located within the center of the ranges. This may be a function of elevation; more analysis would be needed to explore this connection further.

Past research has demonstrated that MODIS snow cover products underestimate snow cover due to vegetation obscuring the ground (Nolin, 2010; Rittger et al. 2013). Previous versions of MOD10A1 also systematically miss patchy snow in the spring melt season, leading to significant underestimates in snow cover (Rittger et al. 2013). It is possible that MOD10A1 is failing to detect snow during the spring melt season in this study, leading to false conclusions about WRF's springtime overestimation of snow cover. The MODIS Snow-Covered Area and Grain Size (MODSCAG) historical data product was created to improve the classification of snow covered pixels in highly vegetated areas or during the melt season (Rittger et al. 2013). MODSCAG uses spectral unmixing to calculate SCF, incorporating more band information from the MODIS sensor than the MOD10A1 NDSI calculation, and has been shown to be a more accurate version of MOD10A1 Version 5 (Rittger et al. 2013).

MODSCAG has been used in previous studies for comparison with WRF (Wrzesien et al. 2015) and was initially considered for this study. However, analyses of MODSCAG SCF showed that data for higher latitude ranges (the Alaska, Brooks, Coast, Mackenzie, and Canadian Rockies ranges) exhibited a striped pattern of missing data during the winter months (Figure 14). While this pattern can likely attributed to limited light in the winter, it made analyses of these ranges near impossible. In the future, performing the same comparison in this study using the latest MODSCAG data would provide a more robust evaluation of WRF SCF trends.

While MOD10A1 may have limitations, it is important to reiterate that it was chosen for this study because it is one of the few SCF data sets available on a daily timescale. As described in the data section, version 6 of MOD10A1, used in this research, addresses many of the issues

highlighted in previous studies (Riggs et al. 2017; Rittger et al. 2013). Analyzing SCF trends of the mountains in this study using both MOD10A1 version 6 and version 5 could provide further insight into both the reliability of MOD10A1 and WRF's SCF trends. Though Rittger et al. (2013) suggested that the empirical relationship used to calculate SCF from NDSI, used in this study, is not a robust indicator of SCF when applied to broad geographic regions, this research assumed that MOD10A1 SCF was erroneously low and instead used a binary classification.

MOD10A1, for all of the reasons described above, does not represent the true snow cover of the eleven ranges analyzed in this study. However, it has been shown to be reasonably accurate (Parajka and Blosch, 2012; Parajka et al. 2006; Simic et al. 2004; Maurer et al. 2002; Klein and Barnett, 2003). In our comparisons of WRF SCF, we assume that MOD10A1 is the truth, and draw our conclusions about WRF SCF trends based on the reliability of MOD10A1. With this assumption, we conclude that WRF does indeed overestimate snow cover in the spring and summer melt season for six different ranges. In the two mountain ranges (Coast and Mackenzie) where WRF underestimates snow cover, the explanation is not immediately clear. Spatially, there is an indication that WRF misclassifies pixels on the boundaries of ranges, while accurately identifying snow cover in the center of ranges. These results suggest that the SCF algorithm utilized by Noah-MP may misclassify pixels in the spring season, when snow melts irregularly across grid cells and snow cover is patchy. For many of the mountain ranges studied here, however, it does a reasonable job (within +/- 5 SCF percentage points) of simulating SCF for most of the water year.

The RCM simulations of mountain snowpack extent presented by Wrzesien et al. (2018) provide a vital source of information about large-scale mountain snowpack resources that is currently difficult or impossible to retrieve from surface monitoring networks or GCMs.

Understanding the accuracy and limitations of these RCM simulations is therefore critical. Given our limited ability to evaluate RCM simulations observationally, satellite remote sensing is a valuable tool for understanding how WRF simulates mountain snowpack over large areas. Wrzesien et al. (2015) and Minder et al. (2016) both compared WRF Noah-MP LSM simulations to MODSCAG remote sensing data and found contrasting results: in the first study, WRF Noah-MP performed generally well in comparison to MODSCAG, while in the second, it systematically underestimated snow. Both of these studies focused on singular mountain regions. The results of this study expand upon the findings of Wrzesien et al. (2015), suggesting that WRF Noah-MP performs generally well for most of the year for not just the Sierra Nevada, but for most mountain ranges in North America. This result is additional evidence for the usefulness of WRF in estimating large-scale mountain snowpack extent. This study also suggests that WRF tends to overestimate mountain snowpack extent in the spring, a finding that should be explored in greater depth in the future. Further analysis using other remotely sensed data sets of snow cover, including MODSCAG, could provide a more complete evaluation of WRF snow cover trends for North American mountain ranges, as well as greater insight into the legitimacy of the observed spring overestimation trends and how WRF Noah-MP may be biased both seasonally and spatially.

References:

Adam, J. C., Hamlet, A. F., & Lettenmaier, D. P. (2009). Implications of global climate change for snowmelt hydrology in the twenty-first century. *Hydrological Processes*, **23**, 962-972.

Barnett, T. P., J. C. Adam, & Lettenmaier, D. P. (2005). Potential impacts of a warming climate on water availability in snow-dominated regions. *Nature*, **438**, 303-309, doi:10.1038/nature04141.

Bjork, R. G., & Molau, U. (2007). Ecology of Alpine Snowbeds and the Impact of Global Change. *Arctic, Antarctic, and Alpine Research*, **39**(1), 34-43.

Dee, D. P., Uppala, S. M., Simmons, A. J., Berrisford, P., Poli, P., Kobayashi, S., Andrae, U., Balmaseda, M. A., Balsamo, G., Bauer, P., Bechtold, P., Beljaars, A. C. M., van de Berg, L., Bidlot, J., Bormann, N., Delsol, C., Dragani, R., Fuentes, M., Geer, A. J., Haimberger, L., Healy, S. B., Hersbach, H., Holm, E. V., Isaksen, L., Kallberg, P., Kohler, M., Matricardi, M., McNally, A. P., Monge-Sanz, B. M., Morcrette, J.-J., Park, B.-K., Peubey, C., de Rosnay, P., Tavolato, C., Thepaut, J.-N., & Vitart, F. (2011). The ERA Interim reanalysis: configuration and performance of the data assimilation system. *Quarterly Journal of the Royal Meteorological Society*, **137**(656).

Dozier, J., Bair. E. H., & Davis, R. E. (2016). Estimating the spatial distribution of snow water equivalent in the world's mountains. *WIREs Water*, **3**, 461-474. doi:10.1002/wat2.1140

Dudhia, J. (1989). Numerical Study of Convection Observed during the Winter Monsoon Experiment Using a Mesoscale Two-Dimensional Model. *Journal of the Atmospheric Sciences*.

Etchevers, P., Martin, E., Brown, R., Fierz, C., Lejeune, Y., Bazile, E. (2004). Validation of the energy budget of an alpine snowpack simulated by several snow models (SnowMIP project). *Annals of Glaciology*, **38**, 150-158.

Gergel, D. R., Nijssen, B., Abatzoglou, J. T., & Lettenmaier, D. P. (2017). Effects of climate change on snowpack and fire potential in the western USA. *Climatic Change*, **141**(2).

Hall, D. K., & Riggs, G. A. (2011). Normalized-difference snow index (NDSI). *Encyclopedia of Snow, Ice and Glaciers, Encyclopedia of Earth Sciences Series.* 779-780. doi: http://dx.doi.org/10.1007/978-90-481-2642-2_376.

Hall, D. K., Riggs, G. A., Salomonson, V. V., DiGirolamo, N. E., & Bayr, K. J. (2002). MODIS Snow-Cover Products. *Remote Sensing of Environment*, **83**.

Hall, D. K. & Riggs, G. A. (2016). MODIS/Terra Snow Cover Daily L3 Global 500m Grid, Version 6. NDSI Snow Cover. *NASA National Snow and Ice Data Center Distributed Active Archive Center.* doi: https://doi.org/10.5067/MODIS/MOD10A1.006

IPCC, 2013: *Climate Change 2013: The Physical Science Basis.* Cambridge University Press, 1535 pp., doi:10.1017/CBO9781107415324.

Ikeda, K., Rasmussen, R., Liu, C., Gochis, D., Yates, D., & Chen, F. (2010). Simulation of seasonal snowfall over Colorado. *Atmospheric Research*, **97**(4), 462–477. https://doi org.libproxy.lib.unc.edu/10.1016/j.atmosres.2010.04.010

Kain, J. S. & Fritsch, J. M. (1990). A One-Dimensional Entraining/Detraining Plume Model and Its Application in Convective Parameterization. *Journal of the Atmospheric Sciences*, **47**(23), 2784-2802.

Kain, J. S. & Fritsch, J. M. (1993). Convective Parameterization for Mesoscale Models: The Kain-Fritsch Scheme. In: *The Representation of Cumulus Convection in Numerical Models*. American Meteorological Society.

Kain, J. S. (2004). The Kain–Fritsch Convective Parameterization: An Update. *Journal of Applied Meteorology*, **43**, 170-181.

Kapnick, S., & Hall, A. (2011). Causes of recent changes in western North American snowpack. *Climate Dynamics*, **38**(9-10), 1885-1899.

Kapos, V., Rhind, J., Edwards, M., & Price, M. F. (2000). Developing a map of the world's mountain forest. *Forest in Sustainable Mountain Development: A State of Knowledge Report for 2000.*

Klein, A. G. & Barnett, A. C. (2003). Validation of daily MODIS snow cover maps of the Upper Rio Grande River Basin for the 2000-2001 snow year. *Remote Sensing of Environment*, **86**(2), 162-176.

Maurer, E. P., Rhoads, J. D., Dubayah, R. O., & Lettenmaier, D. P. (2002). Evaluation of the snow-covered area data product from MODIS. *Hydrological Processes*, **17**(1).

Minder, J. R., Letcher, T. W., & Skiles, S. M. (2016). An evaluation of high-resolution regional climate model simulations of snow cover and albedo over the Rocky Mountains, with implications for the simulated snow-albedo feedback. *Journal of Geophysical Research: Atmospheres*, 9069-9088.

Mlawer, E. J., Taubman, S. J., Brown, P. D., Iacono, M. J., & Clough, S. A. (1997). Radiative transfer for inhomogeneous atmospheres: RRTM, a validated correlated-k model for the longwave. *Papers on Climate and Atmospheric Physics*, **102**.

Mote, P. W., Hamlet, A. F., Clark, M. P., & Lettenmaier, D. P. (2005). Declining Mountain Snowpack in Western North America. *Bulletin of the American Meteorological Society*, 39-49.

Musselman, K. N., Molotch, N. P., & Margulis, S. A. (2017). Snowmelt response to simulated

warming across a large elevation gradient, southern Sierra Nevada, California. *The Cryosphere*, **111**, 2847-2866.

NASA. MODIS: About. Available at: https://modis.gsfc.nasa.gov/about/

Niu, G-Y., Z-L., Y., Mitchell, K. E., Chen, F., Ek, M. B., Barlage, M., Kumar, A., Manning, K., Niyogi, D., Rosero, E., Tewari, M., & Xia, Y. (2011). The community Noah land surface model with multiparameterization options (Noah-MP): 1. Model description and evaluation with local-scale measurements. *Climate and Dynamics*, **116**.

Niu, G-Y., & Yang, Y-L. (2004). Effects of vegetation canopy processes on snow surface energy and mass balances. *Journal of Geophysical Research: Atmospheres*, **109**.

Niu, G-Y., & Yang, Y-L. (2007). An observation-based formulation of snow cover fraction and its evaluation over large North American river basins. *Journal of Geophysical Research: Atmospheres*, **112**.

Nolin, A. W. (2010). Recent advances in remote sensing of seasonal snow. *Journal of Glaciology*, **56**(200), 1141-1150.

Painter, T. H., Rittger, K., McKenzie, C., Slaughter, P., Davis, R. E. & Dozier, J. (2009) Retrieval of subpixel snow covered area, grain size, and albedo from MODIS. *Remote Sensing of Environment*, **113**(4), 868–879. doi:10.1016/j.rse.2009.01.001

Parajka, J., Holko, L., Kostka, Z., & Bloschl, G. (2012). MODIS snow cover mapping accuracy in a small mountain catchment – comparison between open and forest sites. *Hydrology and Earth System Sciences*, **16**, 2365-2377.

Parajka, J. & Bloschl, G. (2006). Validation of MODIS snow cover images over Austria. *Hydrology and Earth System Sciences*, **10**(5), 679-689.

Riggs, G. A., Hall, D. K., & Roman, M. O. (2017). Overview of NASA's MODIS and Visible Infrared Imaging Radiometer Suite (VIIRS) snow-cover Earth System Data Records. *Earth System Science Data*, **9**, 765-777.

Riggs, G. A., Hall, D. K., & Roman, M. O. (2016). MODIS Snow Products Collection 6 User Guide. NASA.

Rittger, K., Painter, T. H. & Dozier, J. (2013). Assessment of methods for mapping snow cover from MODIS. *Advances in Water Resources*, **51**, 367–380. doi:10.1016/j.advwatres.2012.03.002

Robinson, D. A., Dewey, K. F., & Heim Jr., R. R. (1993). Global Snow Cover Monitoring: An Update. *Bulletin of the American Meteorological Society*, 1689-1696.

Salomonson, V. V. & Appel, I. (2004). Estimating fractional snow cover from MODIS using the

normalized difference snow index. *Remote Sensing of the Environment*, **89**(3), 351-360.

Simic, A., Fernandes, R., Brown, R., Romanov, P., & Park, W. (2004). Validation of VEGETATION, MODIS, and GOES+SSM/I snow cover products over Canada based on surface snow depth observations. *Hydrological Processes*, **18**, 1089–1104.

Skamarock, W. C., Klemp, J. B., Dudhia, J., Gill, D. O., Barker, D. M. & Duda, M. G. (2008). A description of the advanced research WRF version 3. *Technical Note 475*. Boulder, CO: National Center for Atmospheric Research.

Sun, F., Berg, N., Hall, A., Schwartz, M. & Walton, D. (2018). Understanding End-of-Century Snowpack Changes Over California's Sierra Nevada. *Geophysical Research Letters*, **46**(2).

Stewart, T. I. (2009). Changes in snowpack and snowmelt runoff for key mountain regions. *Hydrological Processes*, **23**, 78-94. doi:10.1002/hyp.7128

Thompson, G., Rasmussen, R. M., & Manning, K. (2004). Explicit Forecasts of Winter Precipitation Using an Improved Bulk Microphysics Scheme. Part I: Description and Sensitivity Analysis. *American Meteorological Society Monthly Weather Review*.

Viviroli, D., H. H. Durr, B. Messerli, M. Meybeck, & Weingartner, R. (2007). Mountains of the world, water towers for humanity: Typology, mapping, and global significance. *Water Resources Research*, **43**, W07447, doi:10.1029/2006WR005653.

Westerling, A. L., Hidalgo, H. G., Cayan, D. R., & Swetnam, T. W. (2006). Warming and Earlier Spring Increase Western U.S. Forest Wildfire Activity. *Science*, **313**, 940-943.

Wrzesien, M. L., Pavelsky, T. M., Kapnick, S. B., Durand, M. T., & Painter, T. H. (2014). Evaluation of snow cover fraction for regional climate simulations in the Sierra Nevada. *International Journal of Climatology*, **35**(9).

Wrzesien, M. L., Durand, M. T., Pavelsky, T. M., Howat, I. M., Margulis, S. A. & Huning, L. S. (2017). Comparison of methods to estimate snow water equivalent at the mountain range scale: a case study of the California Sierra Nevada. *Journal of Hydrometeorology*, **18**, 1101-1119, doi:10.1175/JHM-D-16-0246.1.

Wrzesien, M. L., Durand, M. T., Pavelsky, T. M., Kapnick, S. B., Zhang, Y., Guo, J. & Shum, C. K. (2018). A new estimate of North American mountain snow accumulation From regional climate model simulations. *Geophysical Research Letters*, **45**, 1423-1432, doi:10.1002/2017GL076664

Zeng, X., Broxton, P. & Dawson, N. (2018). Snowpack Change From 1982 to 2016 Over Conterminous United States. *Geophysical Research Letters*, **45**(23).

Appendix

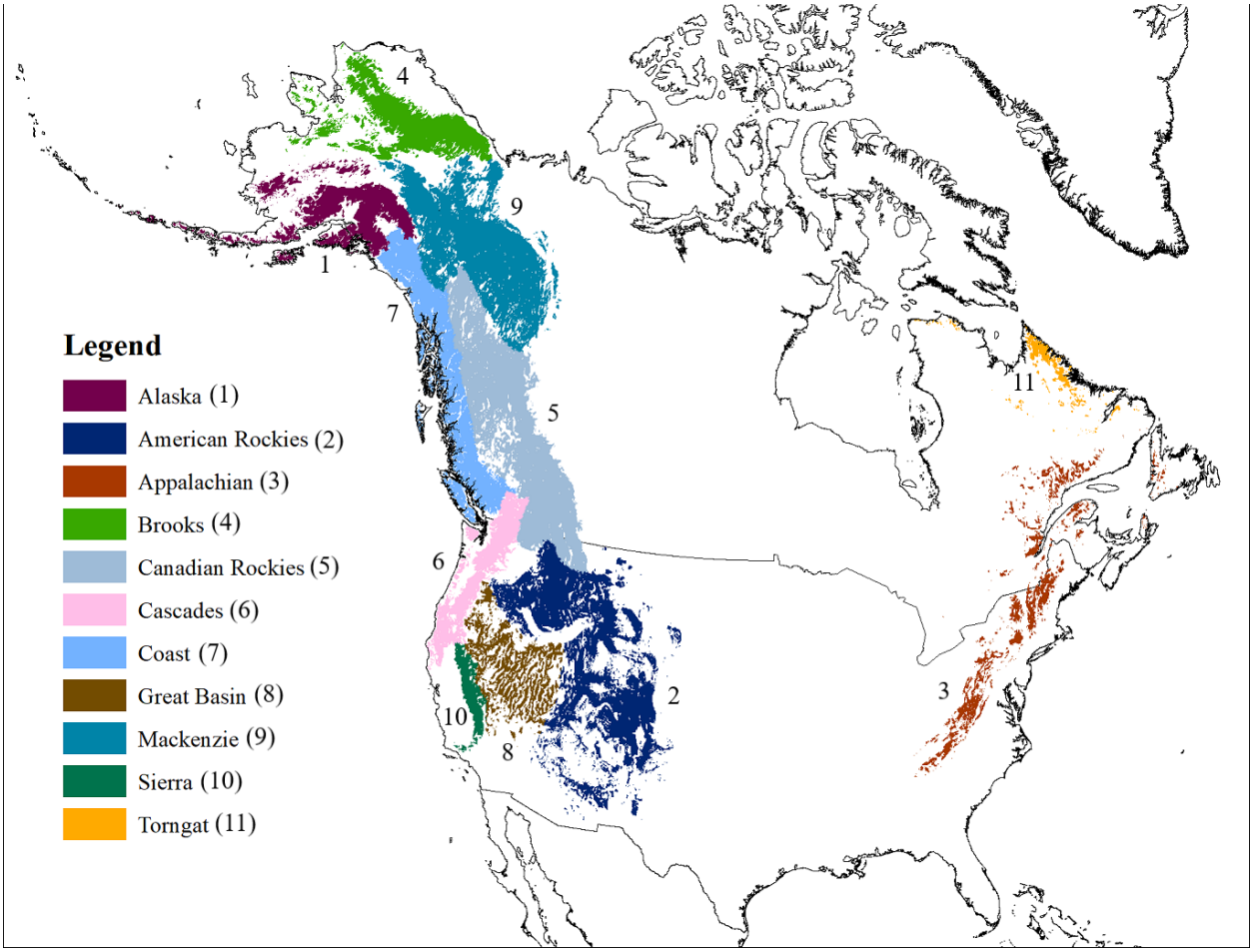

Figure 1. Map of spatial extents of North American mountain ranges.

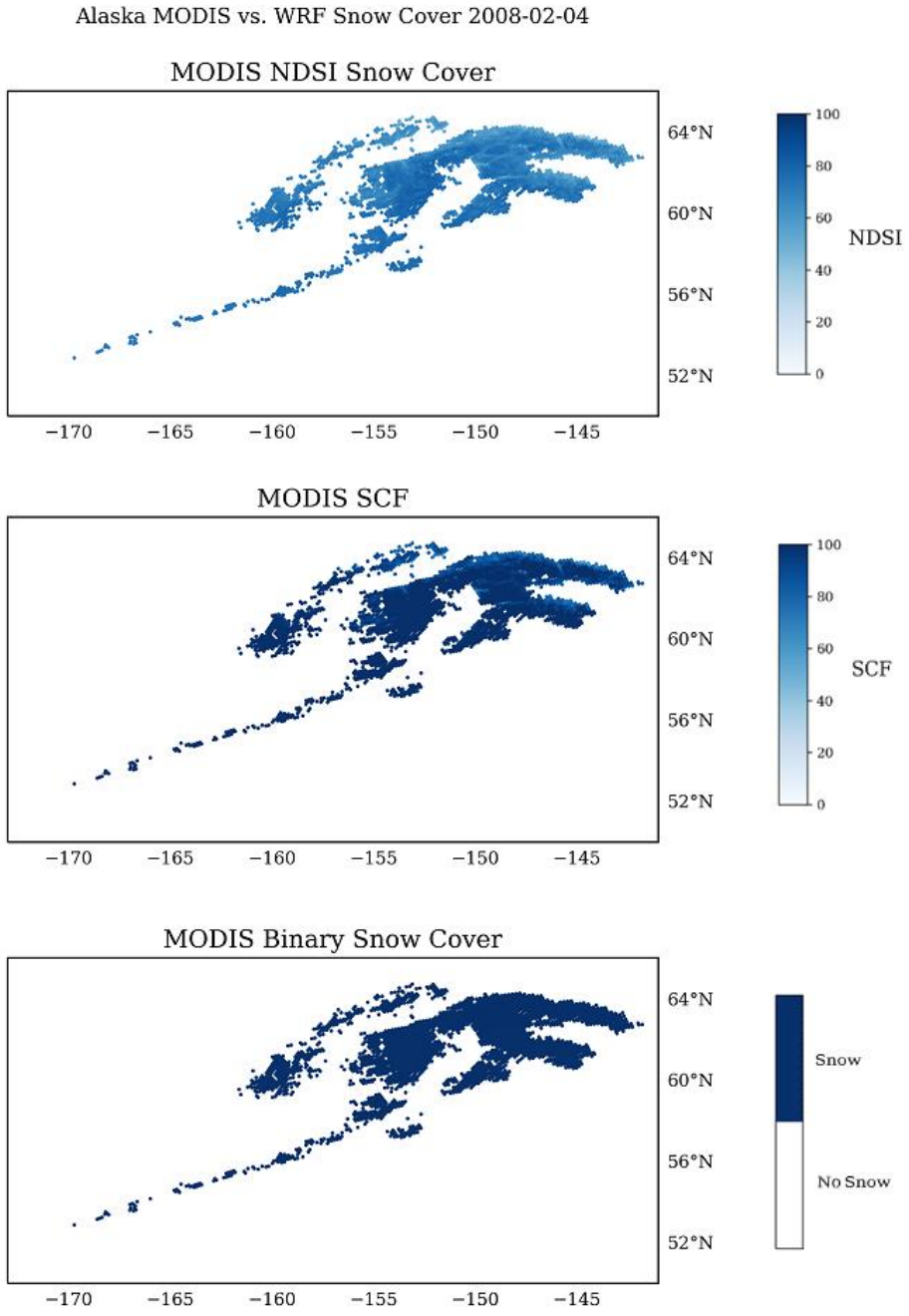

Figure 2. MODIS NDSI snow cover, on the top, compared to a binary snow classification ('snow', 'no snow') of 0.15 SCF, on the bottom, for the Alaska range in early February.

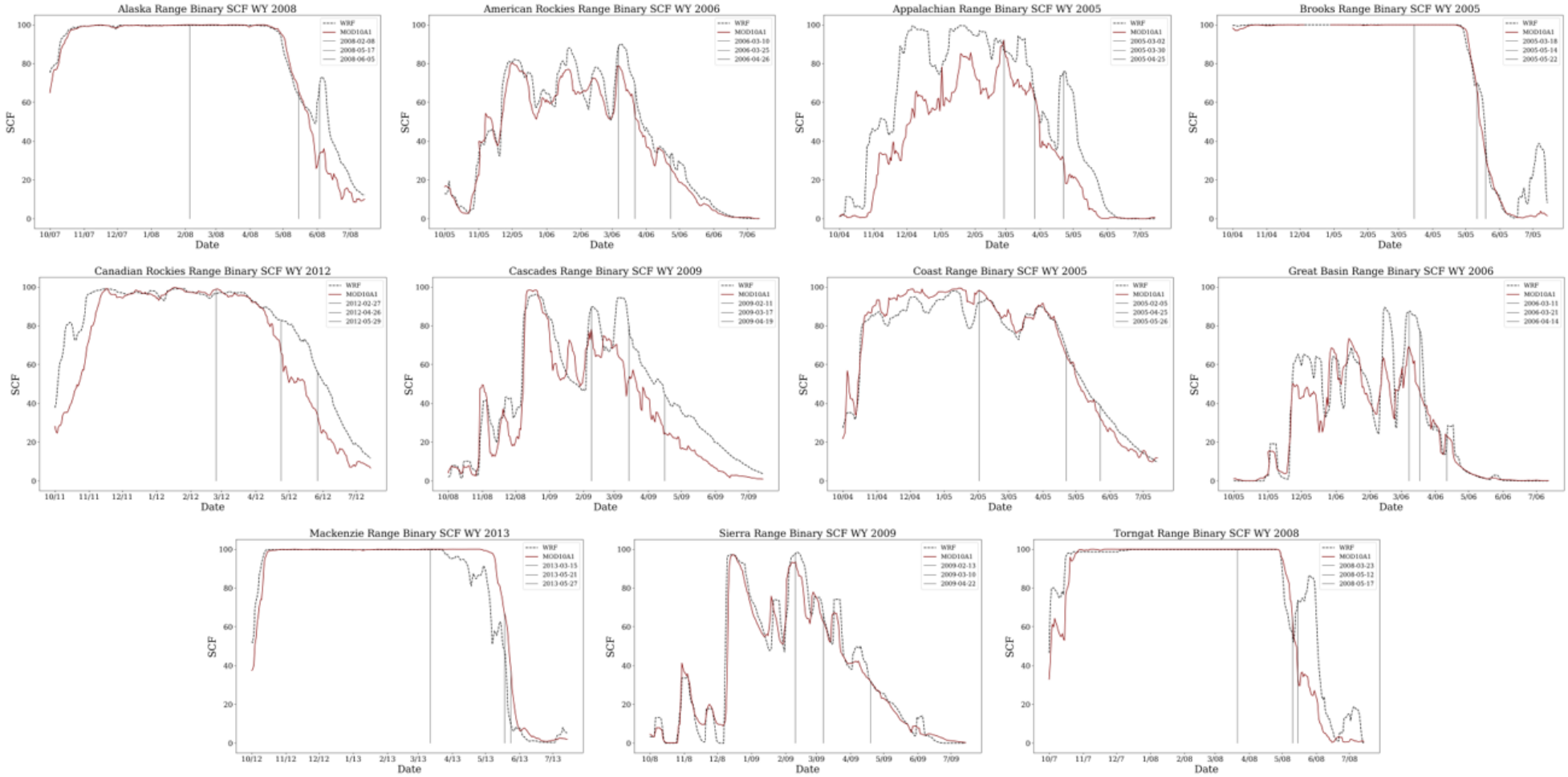

Figure 3. Time series graphs for each range comparing WRF estimates of binary SCF to MOD10A1 for every day of the respective water year. Early-, mid-, and late-season dates are shown with black lines.

Alaska

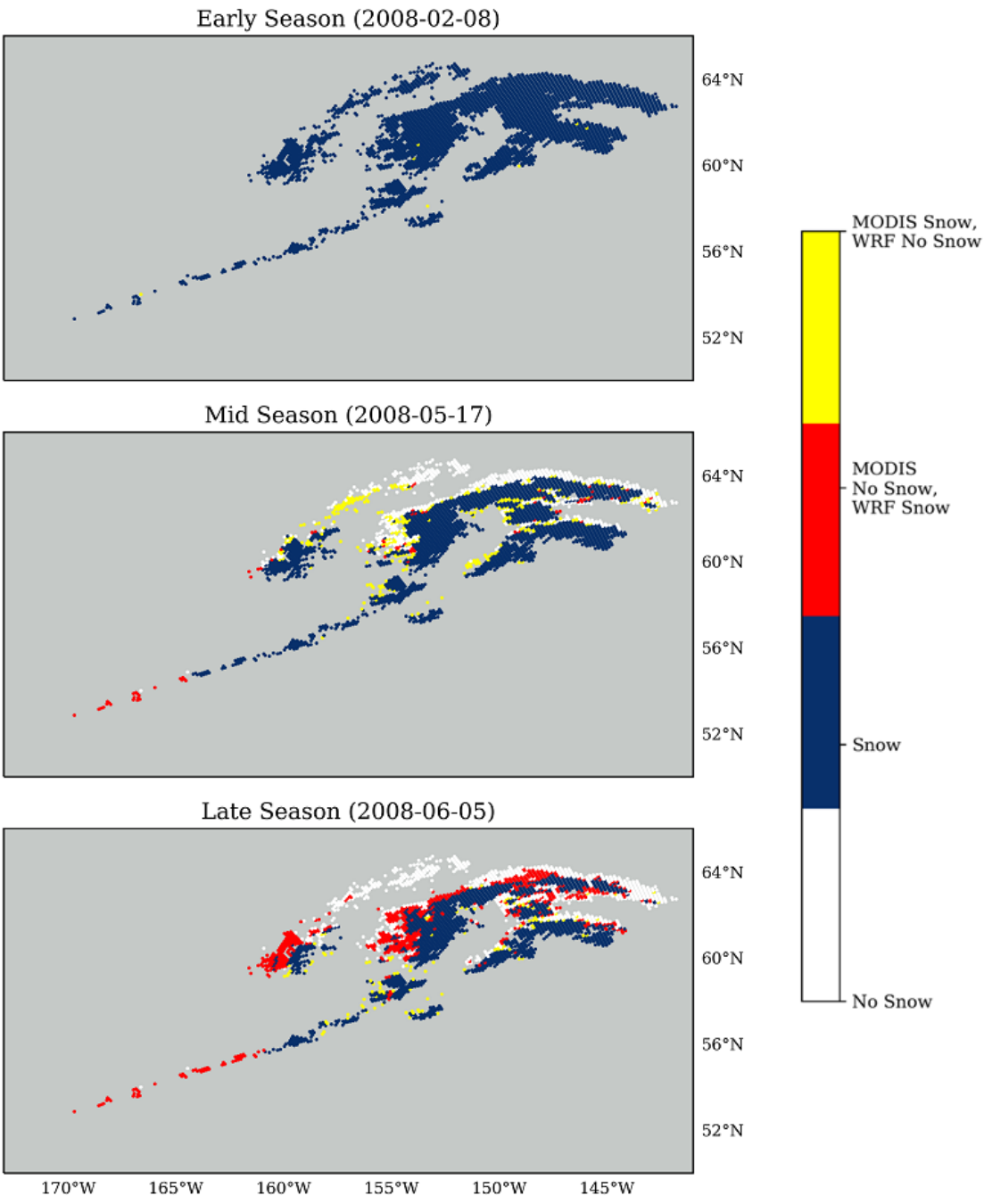

Figure 4. Alaska WRF vs. MODIS binary SCF for early-, mid-, and late-season dates.

American Rockies

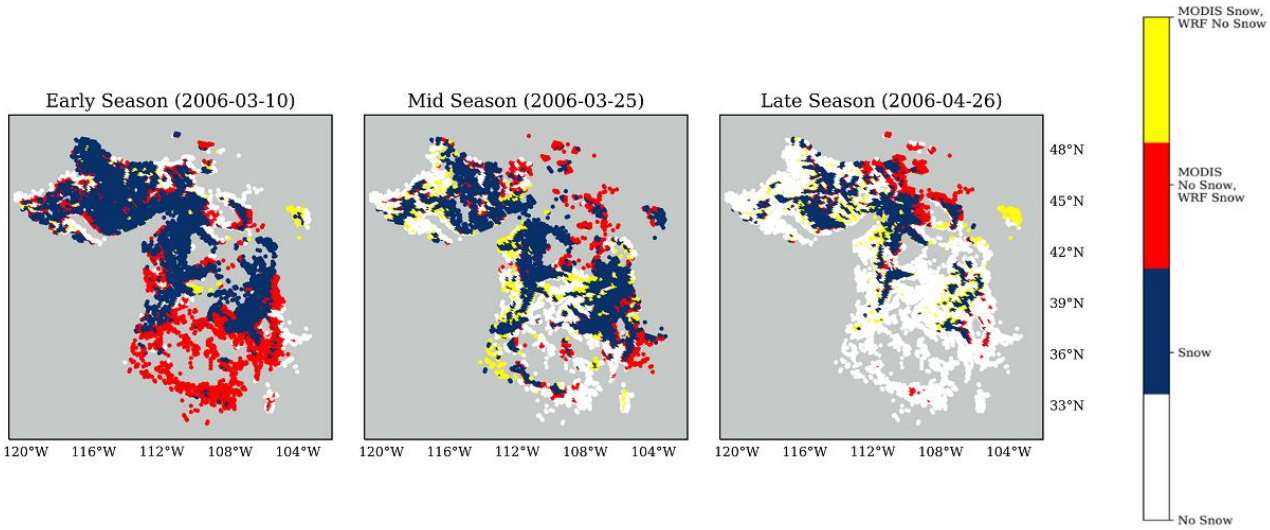

Figure 5. American Rockies WRF vs. MODIS binary SCF for early-, mid-, and late-season dates.

Appalachian

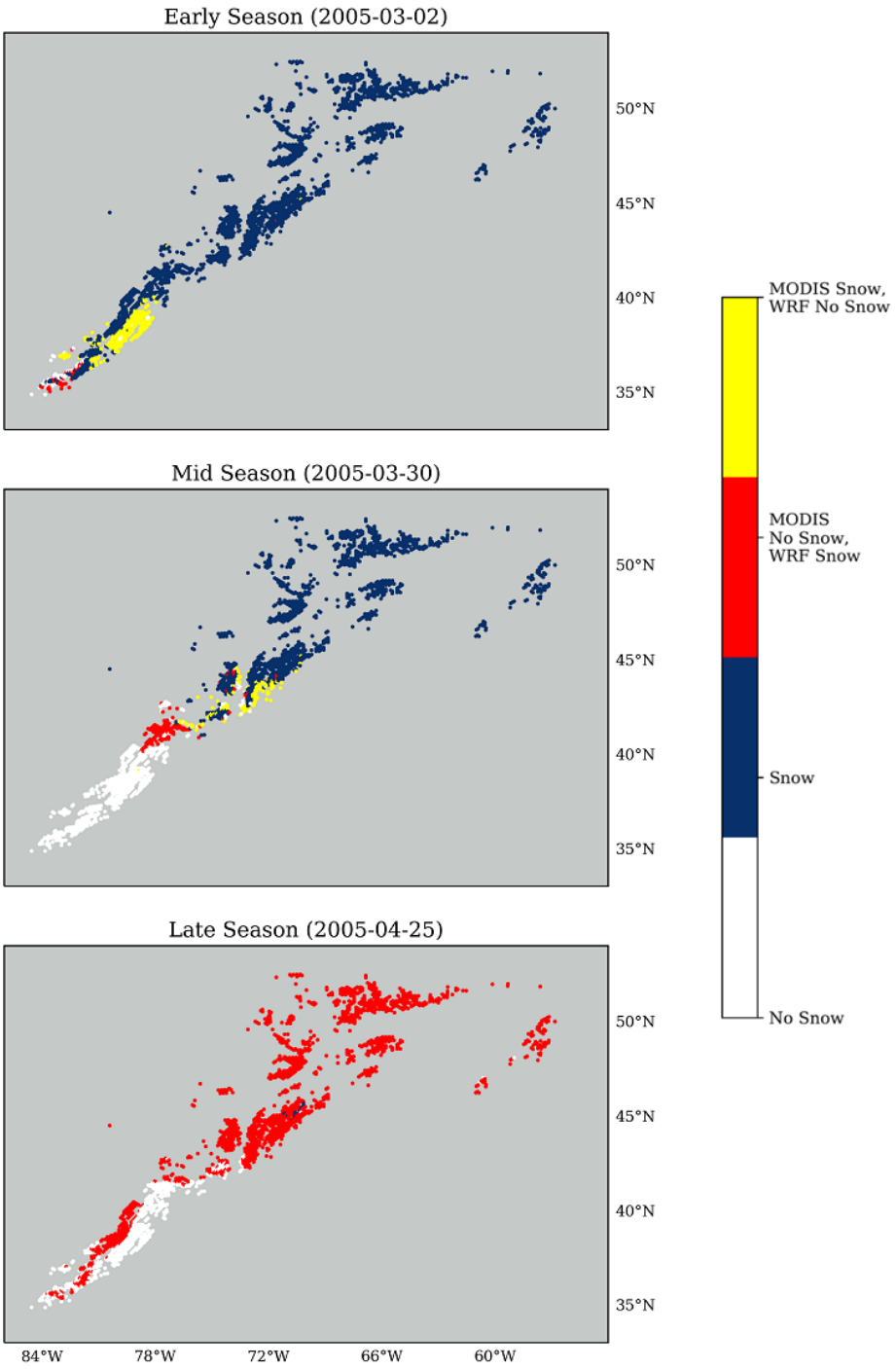

Figure 6. Appalachian WRF vs. MODIS binary SCF at early-, mid-, and late-season dates.

Brooks

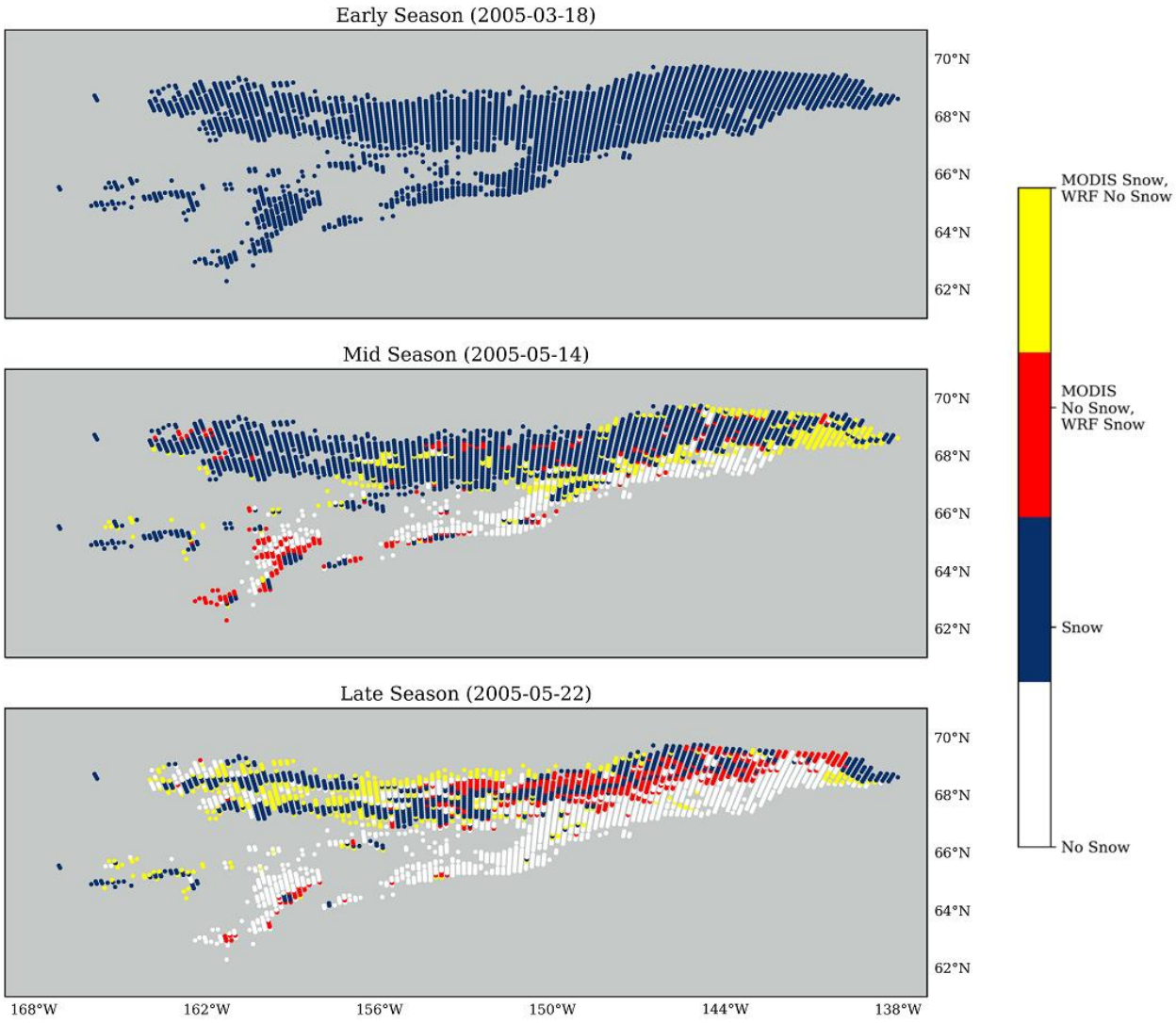

Figure 7. Brooks WRF vs. MODIS binary SCF for early-, mid-, and late-season dates.

Canadian Rockies

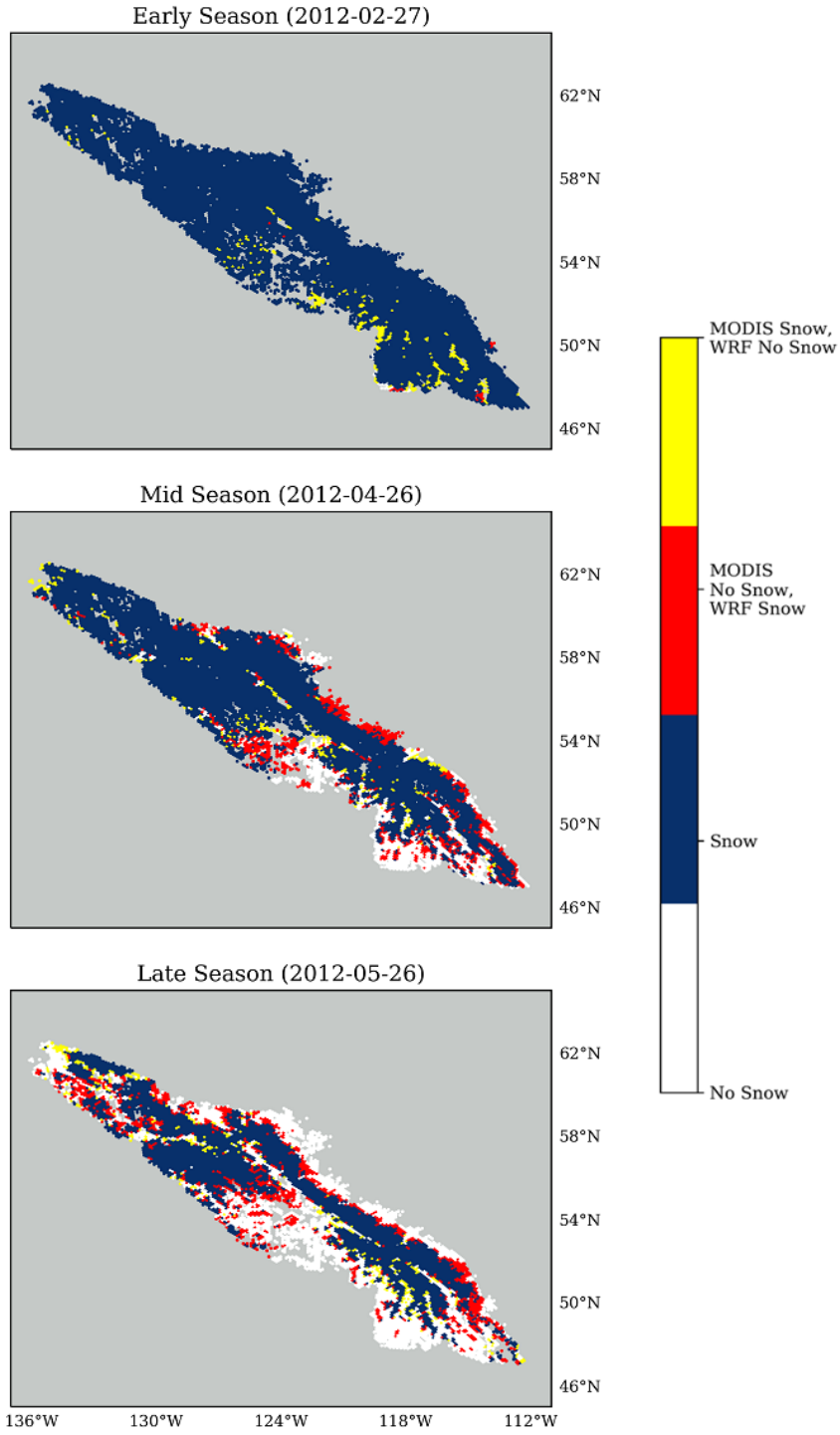

Figure 8. Canadian Rockies WRF vs MODIS binary SCF for early-, mid-, and late-season dates.

Cascades

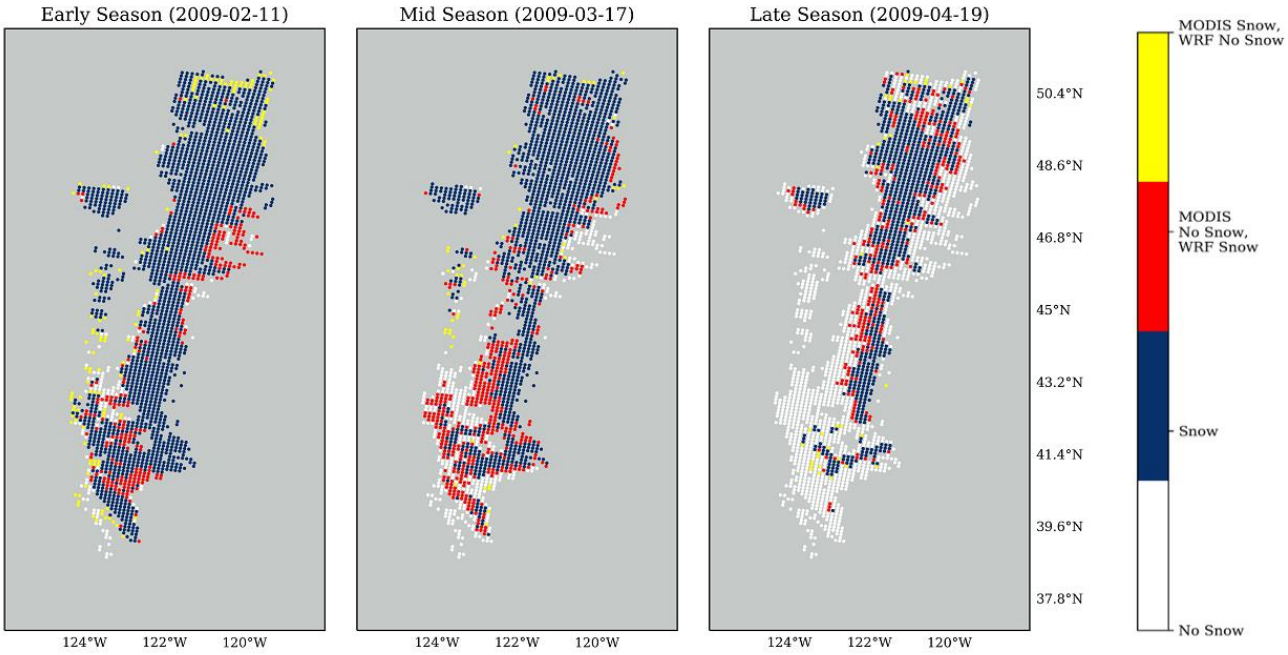

Figure 9. Cascades WRF vs. MODIS binary SCF for early-, mid-, and late-season dates.

Coast

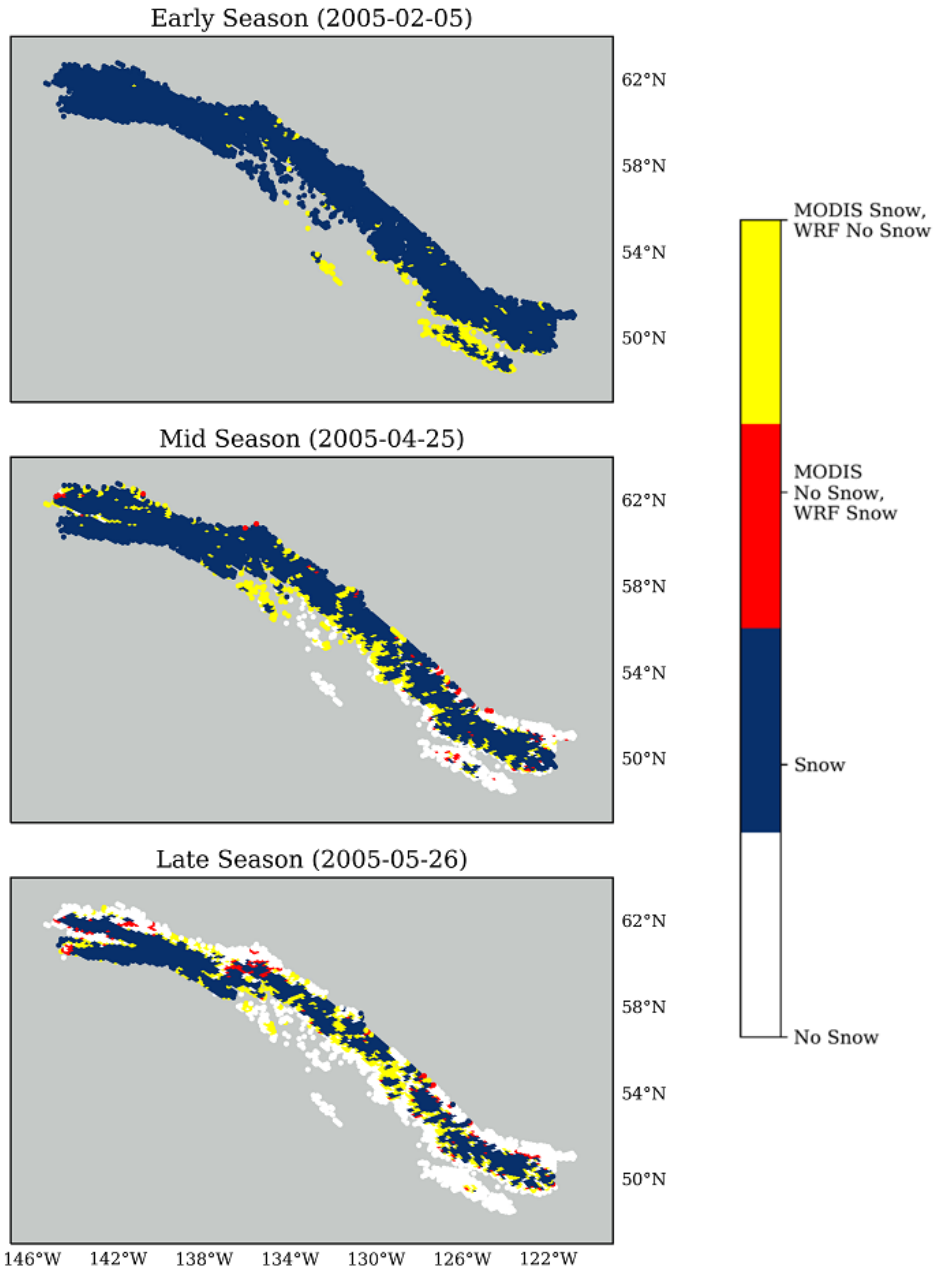

Figure 10. Coast WRF vs MODIS binary SCF for early-, mid-, and late-season dates.

Great Basin

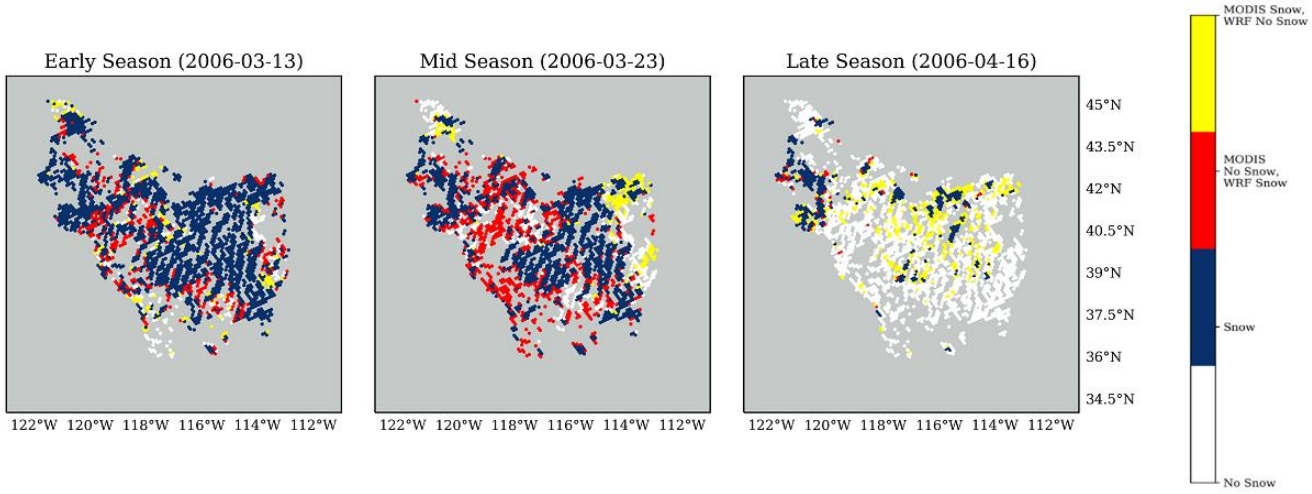

Figure 11. Great Basin WRF vs MODIS binary SCF for early-, mid-, and late-season dates.

Mackenzie

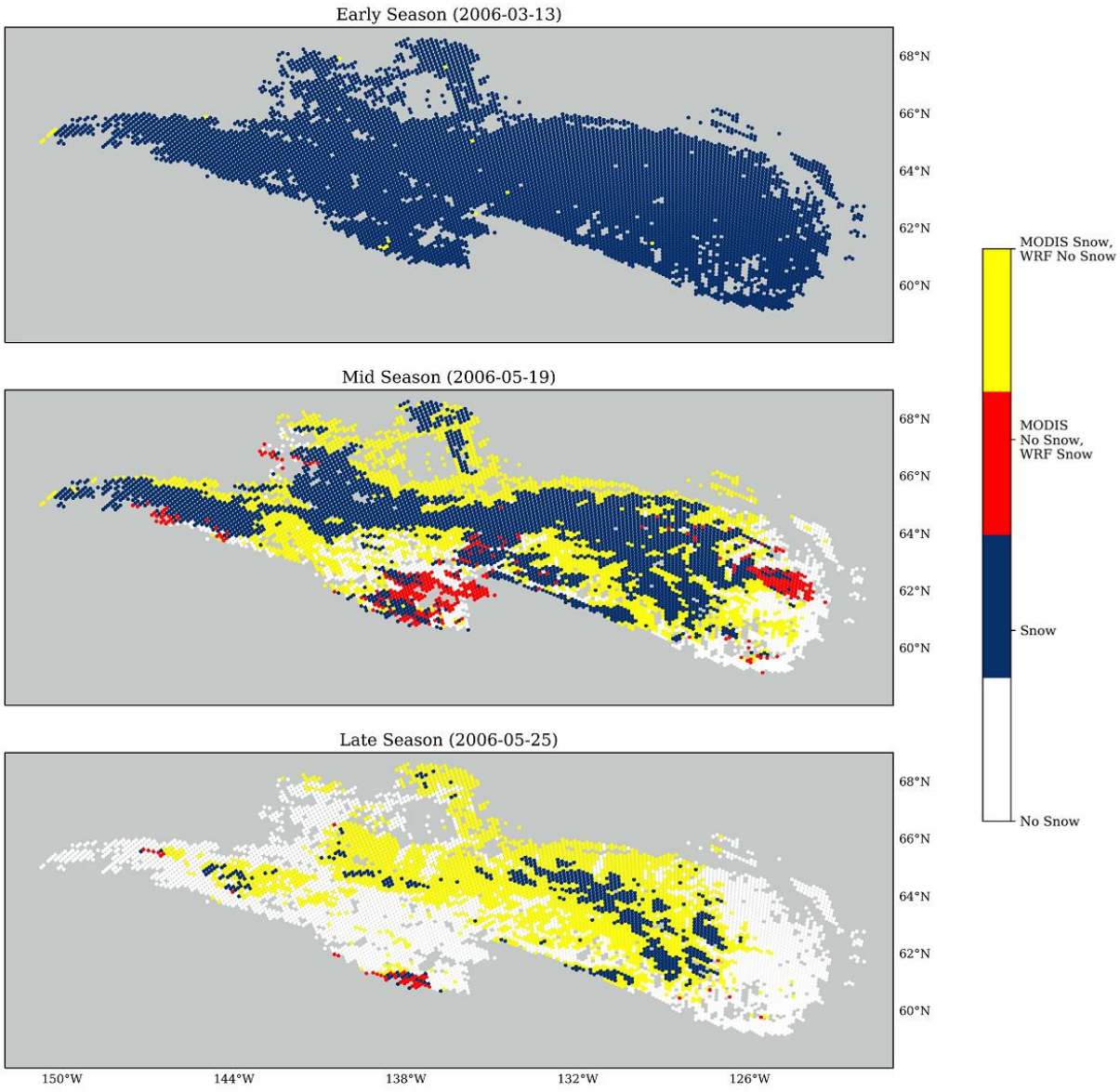

Figure 12. Mackenzie WRF vs. MODIS binary SCF for early-, mid-, and late-season dates.

Sierra

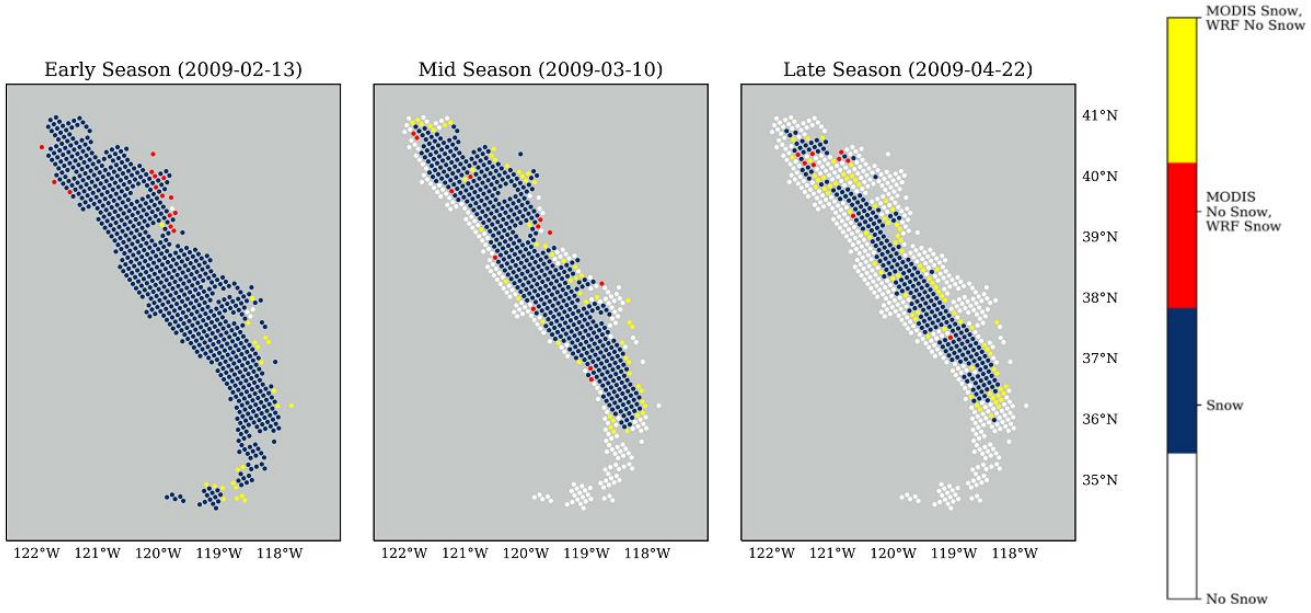

Figure 13. Sierra WRF vs MODIS binary SCF for early-, mid-, and late-season dates.

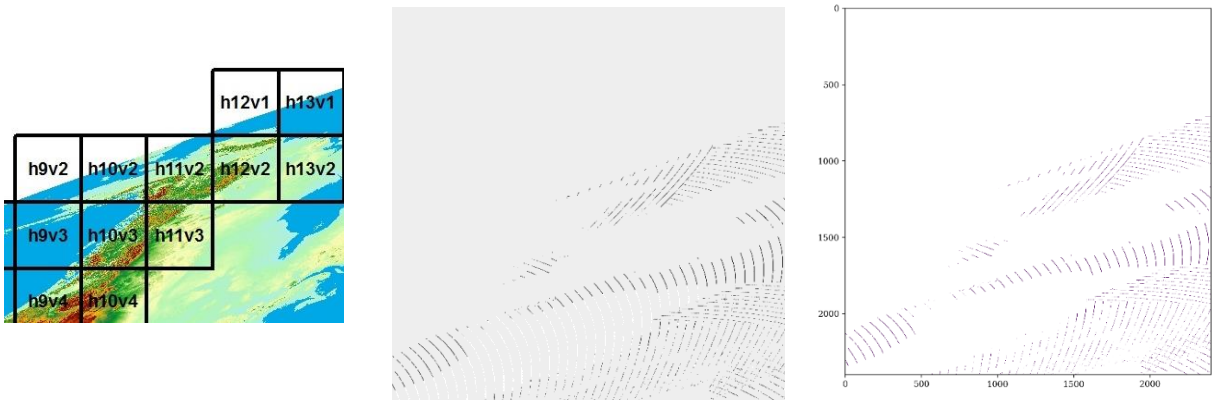

Figure 14. MODSCAG tile h10v02, representing Alaska, for January 1st, 2004. (A) shows the geographic extent of the MODSCAG tiles, with h10v02 shown on the second row (map produced by Karl Rittger), (B) is the raw tif file, and (C) is the processed tile, with any SCF values between 0-100 shown.

	Early Season				Mid Season				Late Season			
Range	TN	FP	FN	TP	TN	FP	FN	TP	TN	FP	FN	TP
Alaska	0	0	0	100	20	3	11	66	26	22	4	48
American Rockies	10	26	2	62	27	10	10	53	59	7	8	26
Appalachian	2	2	10	86	30	6	5	59	24	75	0	1
Brooks	0	0	0	100	18	7	14	61	45	15	15	25
Canadian Rockies	0	0	3	97	14	11	3	72	36	15	4	45
Cascades	6	11	6	77	17	20	2	61	54	12	2	32
Coast	0	0	6	94	13	2	12	73	35	4	14	47
Great Basin	8	22	4	66	15	23	6	56	73	4	12	11
Mackenzie	0	0	0	100	13	4	31	52	40	0	45	15
Sierra	0	2	3	95	26	2	7	65	59	1	9	31

Table 1. Percentage of pixel classifications by WRF and MODIS for each range at the early-, mid-, and late-season dates. TN (true positive) refers to pixels classified as no snow by both WRF and MOD10A1. FP (false positive) are pixels classified as snow by WRF and no snow by MOD10A1. FN (false negative) are pixels classified as no snow by WRF and snow by MOD10A1. TP (true positive) are pixels classified as snow by both datasets.